DELFT UNIVERSITY OF TECHNOLOGY

REPORT 04-01

On Rain-wind Induced Vibrations of a Seesaw Oscillator

Hartono and W.T. van Horssen

ISSN 1389-6520

Reports of the Department of Applied Mathematical Analysis

Delft 2004

On Rain-wind Induced Vibrations of a Seesaw Oscillator

Hartono and W. T. van Horssen

Abstract

In this paper the rain-wind induced vibrations of a seesaw oscillator will be studied. The model equations will be derived under the assumption that the position of the rivulet of water on the oscillator varies in time. The eigenfrequency of the oscillator and the frequency of the movement of the water rivulet on the oscillator are assumed to be close to each other. Several Hopf and saddle node bifurcations will occur when the amplitude of the movement of the water rivulet on the oscillator is varied.

1 Introduction

There are many examples of rain-wind induced vibrations of elastic structures such as cables or bridges. The Erasmus bridge in Rotterdam and the Meikonishi bridge in the Nagoya Harbor in Japan are examples of such elastic structures. The cables of these bridge are stable under dry wind condition (no rain), but can become unstable when it is raining (see also [3]). Another instability mechanism can be caused by torsional flutter as for instance described in [6]. This instability mechanism might have been the cause of the collapse of the Tacoma Narrows bridge. The first instability mechanism can be described by spring type oscillators, and the torsional instability mechanism can be modelled by seesaw type oscillators (see also [1, 2]). In [1, 2] a rather complete analysis of the vibrations of a spring type oscillator and of a seesaw type oscillator with a fixed position of the water-rivulet on the oscillators has been presented. And in [9] an analysis for the spring oscillator has been given when the position of the water ridge on the oscillator varies in time.
In this paper the vibrations of a seesaw oscillator with a time-varying position of a water ridge on the surface of the oscillator will be studied. In Figure 1 a sketch is given of the circular cross-section of the seesaw oscillator with such a water ridge (in black) on the surface. In fact the seesaw oscillator consists of a circular cylinder connected to a rigid bar. At the other end of the bar a hinge-axis is connected such that the bar-cylinder can rotate around this axis (see also Figure 1). It is assumed that for each cross-section of the cylinder the time-varying position of the water ridge is the same.
This paper is organized as follows. In section 2 the equations describing the vibrations of the seesaw oscillator will be derived. In section 3 and in section 4 the effect of the

amplitude of the variation in the position of the water rivulet will be studied for different values of the parameters. Finally in section 5 some conclusions will be drawn.

2 Derivation of the equation of motion

The angle θ, measured positive in clockwise direction, describes the angle between the arm holding the cylinder and the horizontal line. The angle α_s denotes the angle between the rotation arm and a symmetry axis of the cylinder's cross-section, counted positive in clock wise direction, see Figure 1. Further, R is the distance from the cylinder's axis to the pivot O. It is assumed that a quasi-steady theory can be used to model the windforces acting on the cylinder. The quasi-steady theory implies that for the description of the dynamics of the elastic structure with the flowing medium one may use data which describes the static situation. More precisely one assumes that the fluid forces on the structure are determined solely by the instantaneous resultant flow velocity [1, 8]. The aerodynamic moment M exerted on the structure can be modeled by using the aerodynamic forces exerted on the cylinder. A moment coefficient curve $C_M(\alpha)$ for the structure will be used to describe M.

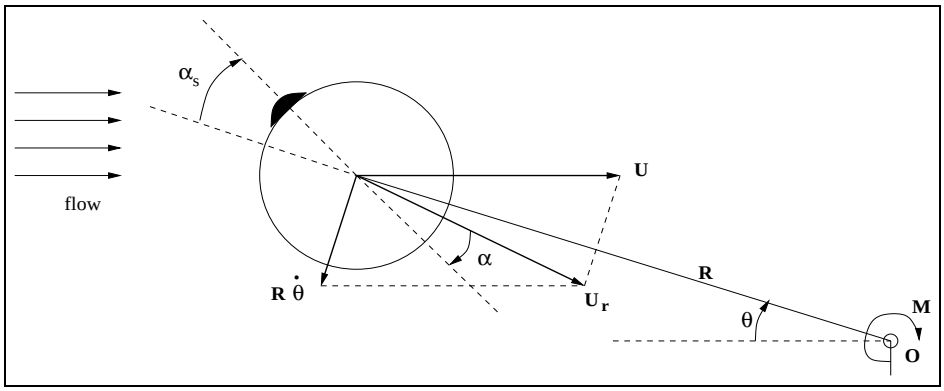

Figure 1: The cross-section of the seesaw oscillator, the fluid flow with respect to the cylinder, and the definitions of the angles α, α_s, and θ.

In the dynamic situation the aerodynamic moment is assumed to be given by

$$M(\alpha) \;=\; \frac{1}{2}\rho\; d\; l\; R\; U_r^2\; C_M(\alpha), \tag{1}$$

where ρ is the density of air, d the diameter of the cylinder, l the length of the cylinder and

$$\alpha \;=\; \alpha_s + \theta - \arctan\left(\frac{R\dot{\theta}\cos\theta}{U - R\dot{\theta}\sin\theta}\right), \tag{2}$$

the angle between the instantaneous velocity vector U_r of the flow relative to the cylinder and the symmetry axis, measured positive in clockwise direction, and

$$U_r^2 \;=\; (U - R\dot{\theta}\sin\theta)^2 + (R\dot{\theta}\cos\theta)^2. \tag{3}$$

The equation of motion is given by :

$$I\ddot{\theta} + c_\theta\dot{\theta} + k_\theta\theta = M(\alpha), \tag{4}$$

where I is the structural moment of inertia, $k_\theta > 0$ the linear torsional spring constant, and $c_\theta > 0$ the structural damping coefficient of the oscillator. Defining the dimensionless parameters $\omega_\theta^2 = k_\theta/I$ and $\mu = U/R\omega_\theta$ and introducing the transformation $\tau = \omega_\theta t$, the following equation is obtained from (4) :

$$\frac{d^2\theta}{d\tau^2} + \frac{c_\theta}{\omega_\theta I}\frac{d\theta}{d\tau} + \theta = \frac{\rho dlR^3}{2I}(\mu^2 - 2\mu\frac{d\theta}{d\tau}\sin\theta + (\frac{d\theta}{d\tau})^2)C_M(\alpha), \tag{5}$$

where $\alpha = \alpha_s + \theta - \arctan(\frac{\frac{d\theta}{d\tau}\cos\theta}{\mu - \frac{d\theta}{d\tau}\sin\theta})$. By assuming that both damping and aerodynamic moments are small, i.e. :

$$\frac{\rho dlR^3}{2I} = \epsilon, \qquad \frac{c_\theta}{\omega_\theta I} = 2\beta_\theta\epsilon, \tag{6}$$

where $0 < \epsilon \ll 1$ it follows from (5) that

$$\frac{d^2\theta}{d\tau^2} + \theta = \epsilon[(\mu^2 - 2\mu\frac{d\theta}{d\tau}\sin\theta + (\frac{d\theta}{d\tau})^2)C_M(\alpha) - 2\beta_\theta\frac{d\theta}{d\tau}]. \tag{7}$$

A similar derivation of this equation also can be found in [1]. As described in [7] the $C_M(\alpha)$ curves may be obtained from wind tunnel experiments, and some typical results obtained from measurements in a wind tunnel are sketched in Figure 2. Now the $C_M(\alpha)$ curves will be approximated by cubical polynomials in α near those values of α for which aerodynamic instabilities occur, that is, near $\alpha = \alpha_o$ for which $C_M(\alpha_o) = 0$. So, it is assumed that

$$C_M(\alpha) \;=\; c_1(\alpha - \alpha_o) + c_3(\alpha - \alpha_o)^3, \tag{8}$$

where $c_1 < 0$ and $c_3 > 0$. Further it is assumed that the position of the water ridge on the

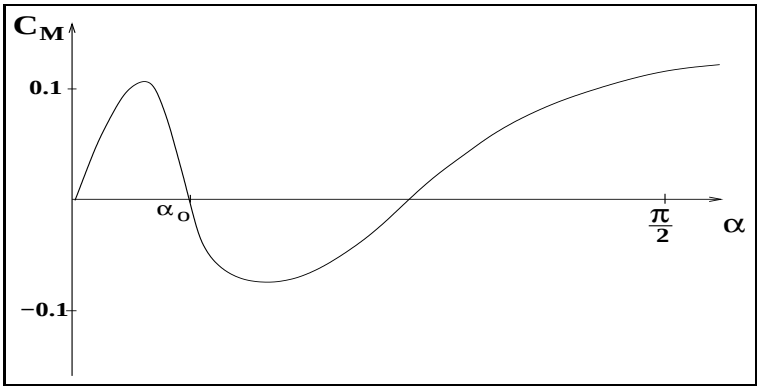

Figure 2: The aerodynamic torsion coefficient $C_M(\alpha)$.

oscillator varies in time according to the following formula

$$\alpha_s - \alpha_o = f(t) = A\cos(\omega t) = A\cos(\frac{\omega}{\omega_\theta}\tau), \tag{9}$$

where A is an amplitude related to the position of the water ridge, and ω is the frequency of the movement of the water ridge. By putting $\frac{\omega}{\omega_\theta} = \Omega = 1 + \epsilon\eta$, where η is a detuning parameter and by introducing the transformation $\Omega\tau = \sigma$ it follows that (7) can be rewritten in

$$\frac{d^2\theta}{d\sigma^2} + \Omega^{-2}\theta = \epsilon[(\frac{\mu^2}{\Omega^2} - 2\frac{\mu}{\Omega}\frac{d\theta}{d\sigma}\sin\theta + (\frac{d\theta}{d\sigma})^2)C_M(\alpha) - 2\frac{\beta_\theta}{\Omega}\frac{d\theta}{d\sigma}] \tag{10}$$

or in

$$\frac{d^2\theta}{d\sigma^2} + \theta = \epsilon[(\mu^2 - 2\mu\frac{d\theta}{d\sigma}\sin\theta + (\frac{d\theta}{d\sigma})^2)C_M(\alpha) - 2\beta_\theta\frac{d\theta}{d\sigma} + 2\eta\theta] + O(\epsilon^2) \tag{11}$$

with

$$\alpha - \alpha_o = A\cos\sigma + \theta - \arctan(\frac{\frac{d\theta}{d\sigma}\cos\theta}{\mu\Omega^{-1} - \frac{d\theta}{d\sigma}\sin\theta}). \tag{12}$$

It should be observed that in (10) and in (11) it has been assumed that the frequency ω of the position of the water ridge on the surface of the oscillator and the frequency ω_θ of the oscillator itself are close to each other. Furthermore, it is assumed that θ and $\frac{d\theta}{d\sigma}$ are small such that (12) can be expanded in a Taylor series in θ and $\frac{d\theta}{d\sigma}$ (around $\theta = 0$ and $\frac{d\theta}{d\sigma} = 0$). Then by substituting (8) into (11) and by setting

$$\begin{aligned} \theta(\sigma) &= y_1(\sigma)\cos(\sigma) + y_2(\sigma)\sin(\sigma), \\ \frac{d\theta(\sigma)}{d\sigma} &= -y_1(\sigma)\sin(\sigma) + y_2(\sigma)\cos(\sigma), \end{aligned} \tag{13}$$

and by using the Taylor expansion of (12) a system of two first order ordinary differential equations for y_1 and y_2 is obtained. In this system for y_1 and y_2 all terms of degree four and higher are neglected. Then, by applying the first order averaging method to the so-obtained equations for y_1 and y_2, one finally obtains

$$\begin{aligned} \dot{\bar{y}}_1 &= \epsilon[(-\mu p_1 - \beta_\theta)\bar{y}_1 - \mu^2 p_1\bar{y}_2 - 2\mu A p_2\bar{y}_1^2 + 2\mu A p_2\bar{y}_2^2 + 2A(p_2 - 3p_5)\bar{y}_1\bar{y}_2 \\ &\quad -\frac{1}{\mu}(p_3 + 3p_4 + \frac{1}{2}p_o(9\mu^2 + 4))\bar{y}_1^3 - (p_3 + 6p_o)\bar{y}_2^3 - (p_3 - 6p_o)\bar{y}_1^2\bar{y}_2 \\ &\quad -\frac{1}{\mu}(p_3 + 3p_4 - \frac{1}{2}p_o(9\mu^2 - 12))\bar{y}_1\bar{y}_2^2] - \epsilon\eta\bar{y}_2, \\ \dot{\bar{y}}_2 &= \epsilon[\mu^2 A p_1 + \mu^2(p_1 + 12p_o)\bar{y}_1 - (\mu(p_1 + 12p_o) + \beta_\theta)\bar{y}_2 \\ &\quad +A(p_2 + 9p_5)\bar{y}_1^2 - A(3p_2 + 3p_5 + 2p_o)\bar{y}_2^2 - 4\mu A(p_2 + p_o)\bar{y}_1\bar{y}_2 + (p_3 + 6p_o)\bar{y}_1^3 \\ &\quad -\frac{1}{\mu}(p_3 + 3p_4 + \frac{1}{2}p_o(9\mu^2 + 20))\bar{y}_2^3 - \frac{1}{\mu}(p_3 + 3p_4 + \frac{1}{2}p_o(27\mu^2 + 6))\bar{y}_1^2\bar{y}_2 \\ &\quad +(p_3 + 18p_o)\bar{y}_1\bar{y}_2^2] + \epsilon\eta\bar{y}_1, \end{aligned} \tag{14}$$

where $\bar{y}_1$ and $\bar{y}_2$ are order ϵ accurate approximations of y_1 and y_2 respectively on time-scales of order $\frac{1}{\epsilon}$, and where

$$p_o = \frac{1}{16}c_3A^2, \quad p_1 = \frac{1}{2}c_1 + \frac{3}{8}c_3A^2, \quad p_2 = \frac{1}{8}c_1 + \frac{3}{8}c_3 + \frac{1}{16}c_3A^2,$$

$$p_3 = \frac{1}{4}c_1 + \frac{3}{8}c_3 + \frac{3}{8}c_3\mu^2, \quad p_4 = \frac{1}{16}c_1\mu^2, \quad p_5 = \frac{1}{8}c_3\mu^2.$$

For a water ridge with a fixed position (that is, for $f(t) \equiv 0$ and so $A = 0$) system (14) can be rewritten in a more simple form by introducing the polar coordinates $\bar{y}_1 = r\cos\varphi$ and $\bar{y}_2 = r\sin\varphi$, yielding

$$\begin{aligned} \dot{r} &= \epsilon r[q_1 - q_2 r^2], \\ \dot{\varphi} &= \epsilon[\eta + \frac{1}{2}\mu^2 c_1 + p_3 r^2], \end{aligned} \tag{15}$$

where $q_1 = -\frac{1}{2}\mu c_1 - \beta_\theta$ and $q_2 = \frac{1}{\mu}(p_3 + 3p_4)$. It is obvious from (15) that a limit cycle will occur when q_1 and q_2 have the same sign. When q_1 and q_2 have different signs it is also obvious that no limit cycles will occur, and that the origin can be the only critical point of (15). In the next two sections the influence of the movement of the water ridge on the surface of the cylinder will be studied for the following two cases : case I with $q_1 < 0$ and $q_2 < 0$ and case II with $q_1 < 0$ and $q_2 > 0$.

3 Case I : $q_1 < 0$ and $q_2 < 0$

In this section the following choice for the parameters has been made $\mu = 1$, $c_1 = -3$, $c_3 = 2$, $\beta_\theta = 1$, $\eta = 0$ or $\eta \neq 0$ and A is a parameter. This choice turned out to be representative for the behaviour of the solution of system (14), that is, for other values of the parameters the behaviour of the solutions is more or less similar. Firstly it is assumed that $\eta = 0$. It is obvious that the number of critical point of (14) is a function of A. By using a Gröbner basis algorithm in the software package Maple the relation between A and the critical points $(\bar{y}_1, \bar{y}_2)$ of system (14) can be determined, and is given in Figure 3. For some values of A the phase portraits of the system (14) are given in Figure 4, where the horizontal axis the $\bar{y}_1$-axis, and the vertical axis is the $\bar{y}_2$-axis. The label S and U in Figure 3 are related to the stable and unstable critical points respectively. Part of the curve in Figure 3a with label U_1 should be combined with that part of the curve in Figure 3b with label U_1 and so on. The end points of each labeled curve are determined by $\frac{d\bar{y}_i}{dA} = \pm\infty$. From Figure 3 and from Figure 4 it can be seen that the number of critical points of system (14) varies when the value of A is varied. In fact for increasing A the following can be observed :

$$(1cp + \text{a stable limit cycle}) \rightarrow 2cp \rightarrow 3cp \rightarrow 4cp \rightarrow 5cp \rightarrow 4cp \rightarrow$$
$$(3cp + \text{a stable limit cycle}) \rightarrow (2cp + \text{a stable limit cycle}) \rightarrow (1cp + \text{a stable limit cycle}),$$

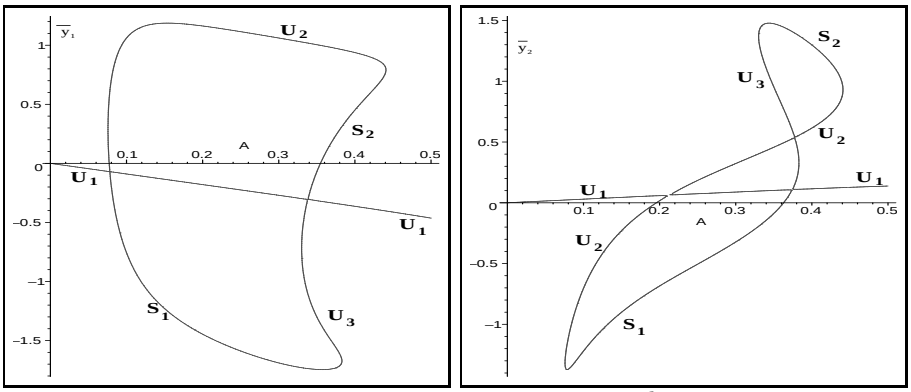

$3a.$ $3b.$

Figure 3: Critical points $(\bar{y}_1, \bar{y}_2)$ of system (14) as function of A, where $\mu = 1$, $c_1 = -3$, $c_3 = 2$, $\beta_\theta = 1$ and $\eta = 0$.

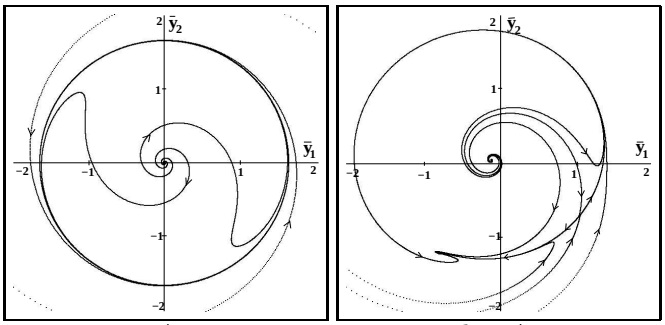

$4a.$ $A = 0$ $4b.$ $A = 0.1$

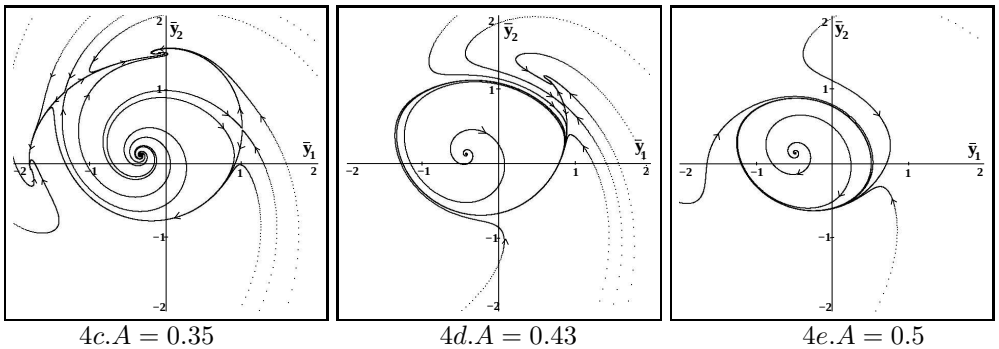

$4c. A = 0.35$ $4d. A = 0.43$ $4e. A = 0.5$

Figure 4: The phase portraits of system (14) for several values of A, and $\mu = 1$, $c_1 = -3$, $c_3 = 2$, $\beta_\theta = 1$ and $\eta = 0$.

where 'cp' is an abbreviation for critical point(s). When $A = 0$ there is one unstable critical point (the origin) and one stable limit cycle. By increasing A the limit cycle will disappear, but for larger values of A it will re-appear. A stable or unstable critical point corresponds with a stable or unstable periodic solution in the original equation (11) and a limit cycle corresponds with a modulated oscillation in the original equation.

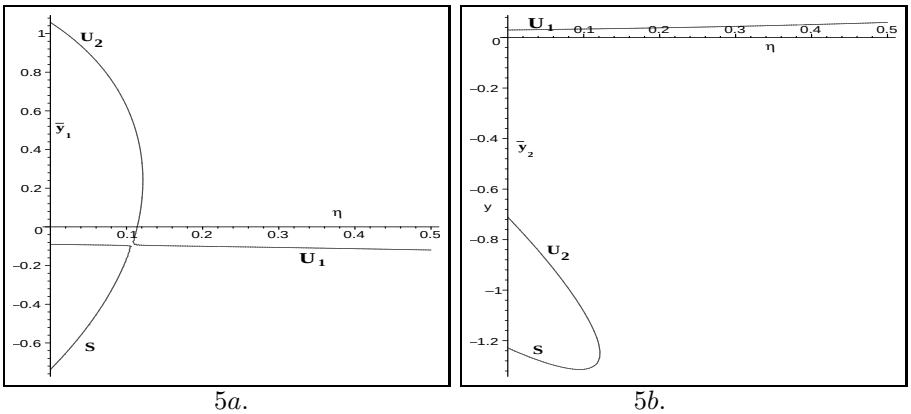

5a. 5b.

Figure 5: Critical points $(\bar{y}_1, \bar{y}_2)$ of system (14) as a function of η, where $\mu = 1$, $c_1 = -3$, $c_3 = 2$, $\beta_\theta = 1$ and $A = 0.1$.

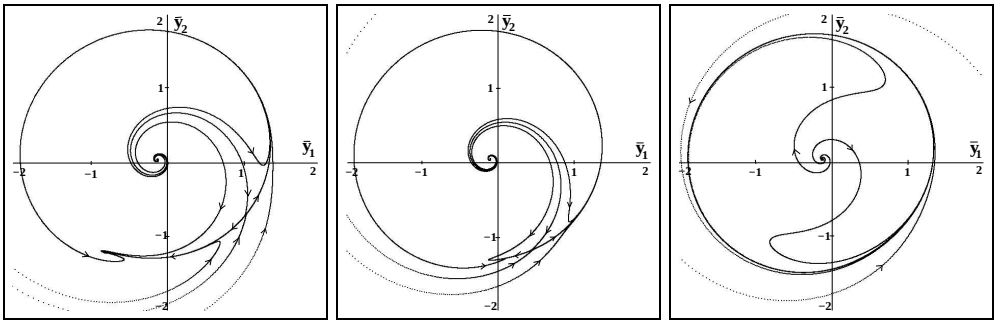

6a. $\eta = 0$ 6b. $\eta = 0.117$ 6c. $\eta = 0.3$

Figure 6: The phase portraits of system (14) for several values of η, where $\mu = 1$, $c_1 = -3$, $c_3 = 2$, $\beta_\theta = 1$ and $A = 0.1$.

Now the effect of the detuning parameter will be studied, and the other parameters are kept fixed, that is, the following choice is made $\mu = 1$, $c_1 = -3$, $c_3 = 2$, $\beta_\theta = 1$, $A = 0.1$ and η is varied. It is obvious that the number of critical points of system (14) will depend on η. Again by using the Gröbner basis algorithm the dependence of the number of critical points on η can be determined and is given in Figure 5. It can be observed from Figure 5 that the number of critical points of system (14) now decreases from 3 to 1 when η increases from 0. The phase portraits of system (14) for several values of η are given in Figure 6. It can be observed from Figure 5 and Figure 6 that a saddle-node bifurcation occurs when the value of η is around 0.125. For smaller values of η there will be 3 critical points, and for larger values there will be one critical point and a limit cycle. For the original equation (11) this implies that for $0 \leq \eta < 0.125$ three periodic solutions will exist (two unstable

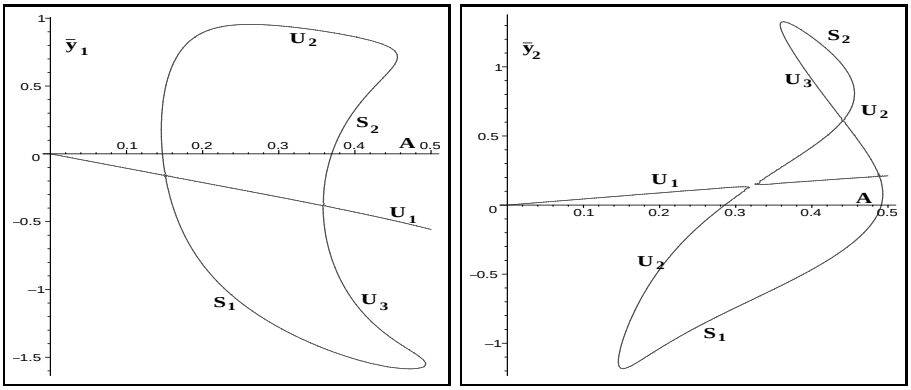

7*a*. 7*b*.

Figure 7: Critical points $(\bar{y}_1, \bar{y}_2)$ of system (14) as a function of A where $\mu = 1$, $c_1 = -3$, $c_3 = 2$, $\beta_\theta = 1$ and $\eta = 0.3$.

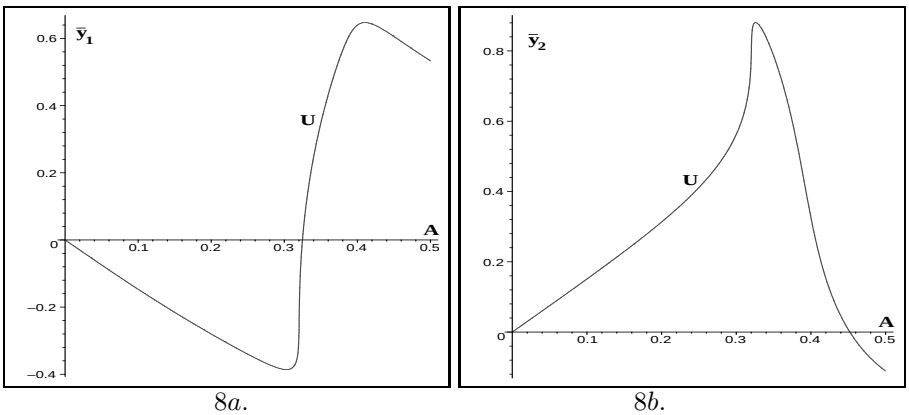

8*a*. 8*b*.

Figure 8: Critical points $(\bar{y}_1, \bar{y}_2)$ of system (14) as a function of A where $\mu = 1$, $c_1 = -3$, $c_3 = 2$, $\beta_\theta = 1$ and $\eta = 1$.

and one stable), that for η approximately equal to 0.125 a stable and an unstable periodic solution will coincide, and that for η larger than 0.125 one unstable periodic solution and a modulated solution will exist. The effect of the detuning parameter η on the positions of the critical points in system (14) can also be seen in Figure 7 and in Figure 8. In Figure 7 η taken to be equal to 0.3, and the results on the position of the critical points can readily be compared with those obtained in Figure 3 for $\eta = 0$.

4 Case II : $q_1 < 0$ and $q_2 > 0$

For $A = 0$ there is only one critical point (stable) of system (14) as has been shown at the end of section 2. In this section the following choice for the parameters has been made $\mu = 1$, $c_1 = -2$, $c_3 = 2$, $\beta_\theta = 2$ and A is a parameter. By using a Gröbner basis algorithm in the software package Maple the relation between A and the critical points $(\bar{y}_1, \bar{y}_2)$ of

system (14) can be determined, and is given in Figure 9 for $\eta = 0$ and in Figure 10 for $\eta = 3$. Also for some values of A the phase portraits of system (14) are given in Figure 11. The results as given in these figures imply that for the given set of parameters only one critical point will occur, which is stable. For the original equation (11) these results imply that a stable periodic solution will exist.

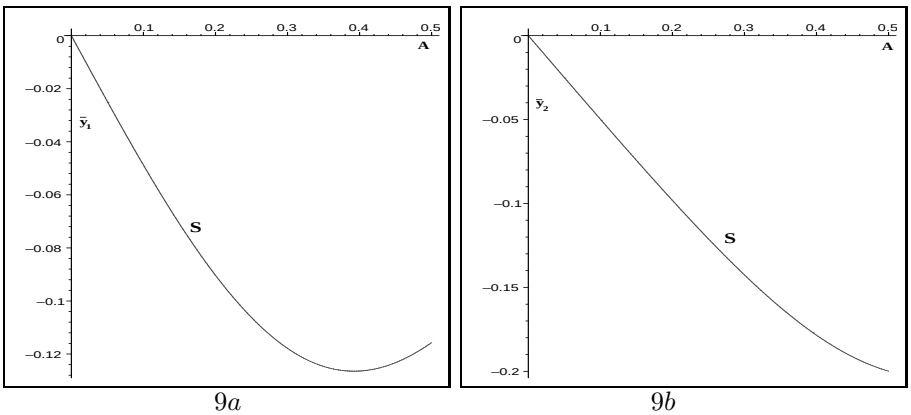

$9a$ $9b$

Figure 9: Critical points $(\bar{y}_1, \bar{y}_2)$ of system (14) as a function of A, where $\mu = 1$, $c_1 = -2$, $c_3 = 2$, $\beta_\theta = 2$ and $\eta = 0$.

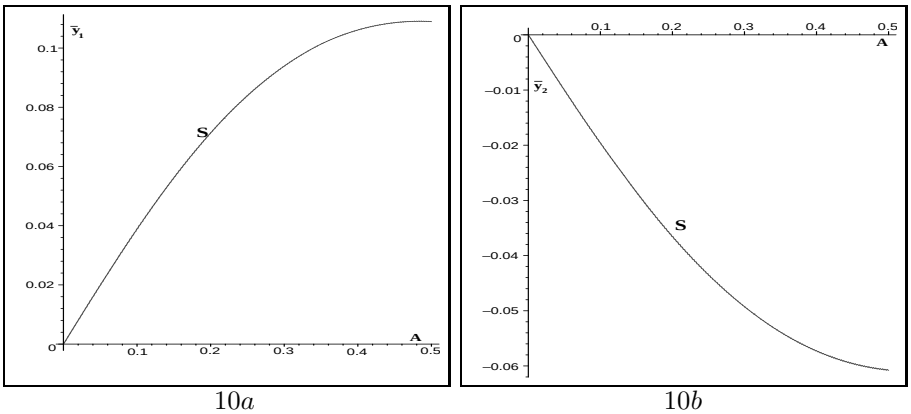

$10a$ $10b$

Figure 10: Critical points $(\bar{y}_1, \bar{y}_2)$ of system (14) as a function of A, where $\mu = 1$, $c_1 = -2$, $c_3 = 2$, $\beta_\theta = 2$, $\eta = 3$.

5 Conclusion

In this paper the rain-wind induced vibration of a seesaw oscillator have been studied. The model equations have been derived under the assumption that the position of the rivulet of water on the oscillator varies harmonically in time. The eigenfrequency of the oscillator

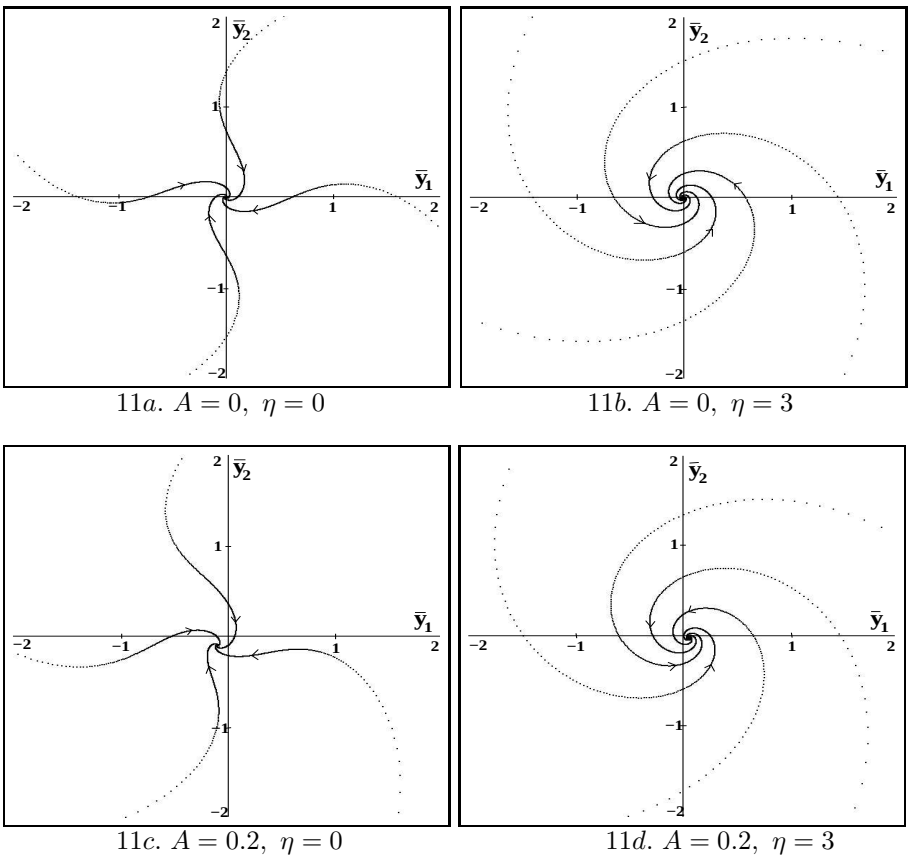

11*a*. $A = 0,\ \eta = 0$ 11*b*. $A = 0,\ \eta = 3$

11*c*. $A = 0.2,\ \eta = 0$ 11*d*. $A = 0.2,\ \eta = 3$

Figure 11: The phase portraits of system (14) for $\mu = 1$, $c_1 = -2$, $c_3 = 2$, $\beta_\theta = 2$, and for different values of A and η.

and the frequency of the movement of the water rivulet on the oscillator are assumed to be close to each other. Several Hopf and saddle-node bifurcations occur when the amplitude of the movement of the water rivulet on the oscillator is varied. For some sets of the parameters in the model equations the existence and the stability of the periodic or of the modulated vibrations have been established.

References

[1] Haaker,T.I., *Quasi-steady Modelling and Asymptotic Analysis of Aeroelastic Oscillators* , PhD thesis, Delft University of Technology, 1996.

[2] Haaker,T.I. and van der Burgh, A.H.P., "On the dynamics of aeroelastic oscillators with one degree of freedom, *SIAM J. Appl. Math.* , Vol. **54**, pp. 1033-1047, 1994.

[3] Hikami, Y. and Shiraishi, N., "Rain-wind induced vibrations of cables in cable stayed bridges", *Journal of Wind Engineering and Industrial Aerodynamics* Vol. 29, pp. 409-418, Elsevier Science Publishers B.V., Amsterdam, 1988.

[4] Matsumoto, M., Shiraishi, N., Kitazawa, M., Knisely, C., Shirato, H., Kim, Y. and Tsujii, M., "Aerodynamic behavior of inclined circular cylinders-cable aerodynamics" *Journal of Wind Engineering and Industrial Aerodynamics*, Vol. **33**, pp. 63-72, Elsevier Science Publishers B.V., Amsterdam, 1990.

[5] Matsumoto, M., Yamagishi, M., Aoki, J. and Shiraishi, N., "Various Mechanism of Inclined Cable Aerodynamics", International Association for Wind Engineering Ninth International Conference on Wind Engineering, Vol. **2**, pp. 759-770., New Age International Publishers Limited Wiley Eastern Limited, New Delhi, 1995.

[6] Nakamura, Y. and Mizota, T., " Torsional flutter of rectangular prisms" *ASCE Journal of Engineering Mechanics Division* **101** (1975), p.p. 125.

[7] Van der Beek, C.G.A., *Asymptotic Analysis of Wind-Induced Vibrations* , PhD thesis, Delft University of Technology, 1989.

[8] Van der Burgh, A.H.P., *Nonlinear Dynamics of Structures Excited by Flows: Quasi-steady Modelling and Asymptotic Analysis in Fluid-Structure Interactions in Acoustics*, CISM Courses and Lectures No. 396, Springer Wien New York ISBN 3-211-83147-9, 1999.

[9] Van der Burgh, A.H.P. and Hartono, "Rain-wind Induced Vibrations of a Simple Oscillator", *International Journal of Non-Linear Mechanics*, Vol. **39** (2004), p.p. 93-100.